Research

Seismic Performance of Concrete Reservoirs Considering Soil-Structure-Fluid Interaction under Near- and Far-Field Seismic Excitations

Reza Moallemi [1*], Behnam Mahboubi [2], Parham Bakhtiari [3], Reza Rezaiy [1], Olafurd Manalo [4]

[1] Department of Civil Engineering, Bozorgmehr University of Qaenat, Qaen, Iran.

[2] Department of Civil Engineering, Faculty of Engineering, Kharazmi University, Tehran, Iran.

[3] Department of Civil Engineering, College of Engineering, University of Tehran, Tehran, Iran.

[4] School of Civil and Environmental Engineering, Korea University, Seongbuk-gu, Seoul, Korea.

*Correspondence should be addressed to Reza Moallemi, Department of Civil Engineering, Bozorgmehr University of Qaenat, Qaen, Iran. Tel: +9809028473127; Fax: +98(056)31006000; Email: Rezamoallemi1378@gmail.com

ABSTRACT

The vulnerability of fluid reservoirs in recent earthquakes and locating of Iran in the Alpine-Himalayan seismic belt and the frequent occurrence of destructive earthquakes, as well as the existence of various faults in our country, results in the safe design and analysis of these structures. Seismic excitations in the near range of the fault have different properties compared to the far fault seismic excitations, such as high-frequency content, long periodic pulses in speed-time history, etc. in the near-fault seismic excitations. Therefore, in the present study, the seismic performance of concrete reservoirs was evaluated by considering soil-structure-fluid interaction under near- and far-fault earthquakes. For this purpose, the finite element method was used for numerical simulation by Abacus software. The nonlinear behavior of the bed and the concrete were modeled with the behavioral models of Mohr-Coulomb and damaged plastic concrete, respectively. The Euler–Lagrange element was used to introduce the hydrodynamic pressure of the reservoir fluid, and an infinite element was used to prevent reflection of seismic waves and earthquake energy loss in the boundary around the bed. After analyzing the boundary distance sensitivity and dimensional analysis of the elements while validating the simulation of parametric studies, the present study was conducted for variables such as earthquake frequency contents, field earthquake, reservoir geometry, and different bed hardness and practical results were presented by comparing the results.

Keywords: MATLAB software, crash prediction, two-lane roads, Interactive Highway Safety Design

1. INTRODUCTION

Concrete reservoirs are currently very significant despite the many water resources crises, and according to forecasts, there are many geopolitical problems in the future for water supply [1].On the other hand, due to a large number of faults and the high cost of construction and maintenance of the water reservoirs, these structures should be constructed in the best possible conditions and the right place [2]. Therefore, there have been many studies in this field [3-5]. Fong showed that part of the reservoir fluid under the effect of dynamic excitation had long periodic kinetics called the convective part of the fluid. Another part of the fluid has a rigid oscillation with the reservoir wall, which is called the impulsive part [6]. Hassner (1957) proposed a simple form to estimate the dynamic effects of fluid in a rigid cylindrical or rectangular reservoir under the horizontal motion of earthquake using

an approximation method without the use of partial differential equations and infinite series [7]. Chen and Kianoush, in 2005 and 2006, presented an analytical method called the repetitive method for investigating the dynamic response of concrete reservoirs [8]. Ghaem Maghami and Kianoush, in 2010 and 2011, investigated the dynamic behavior of rectangular ground concrete reservoirs using two-dimensional and three-dimensional finite element methods [9]. In this research, the dynamic analysis of concrete reservoir was performed by finite element modal analysis and time history, and the effect of different elements on dynamic responses was investigated. Razaghi and Eshghi (2008) developed fragility curves for metallic oil storage tanks. They investigated the effect of two variables, including the ratio of height to length of tank and ratio of fluid height to tank height using a nonlinear time history analysis for 10 different earthquake records. Based on the results for the un-anchored metallic oil storage tanks, the increase of the two mentioned ratios increased the level of failure [10]. Haji Mehrabi et al. evaluated the seismic response of tall, medium, and wide cylindrical steel reservoirs using the finite element method by Abaqus software. The results of this study show that increasing the thickness of the tank floor or its wall results in a reduction in the maximum amount of floor uplifting and plastic rotation at the joint. Also, axial and annular (compressive) stresses in un-anchored tanks are always greater than in anchored tanks, whereas the phenomenon of surface waves in the wide anchored and un-anchored tanks with relatively identical geometrical dimensions is approximately similar [11]. Rondon and Gezie developed fragility curves for

metallic oil storage tanks. They investigated the effect of two variables, including the ratio of height to length of tank and ratio of fluid height to tank height using a nonlinear time history analysis for 10 different earthquake records [12]. Mobaraki et al. presented fragility curves for high-capacity metallic fluid storage tanks with concrete bases. They used both CA and IDA methods to determine reservoir fragility curves. The results of this study show a higher probability of failure to the base columns of these reservoirs. Specifically, it can be stated that PGA values ranging from 0.3 to 0.4 determine the probability of column base failure by 80 to 100% [13]. Saha et al. (2015) evaluated the seismic response of groundwater storage tanks with base separator using the RSM performance level model to investigate the uncertainty in seismic separator parameters. For this purpose, they used Monte Carlo simulation to analyze the data and studied the effect of seismic isolator parameters for nonlinear dynamic analysis. They found that uncertainty in seismic separator parameters significantly influenced the maximum response values of fluid storage tanks, leading to a decrease in the amount of failure level for the maximum earthquake acceleration parameter as an earthquake intensity parameter in the fragility curves of these reservoirs [14]. In recent years, the significant advancement of software and numerical methods, the simulation of failure to tanks has also been carried out with considerable accuracy [15-18]. In this study, the seismic performance of concrete tanks was investigated by considering soil–structure–fluid interaction under near and far-field seismic excitations.

2. METHODOLOGY

In the present study, the SI system was used to introduce the materials. The units of this system are presented in Table 1.

Therefore, the output of the analysis results will also be based on the SI system.

Table 1. SI System Units

Variable	Length	Mass	Time	Stress
Unit of measurement	**Meter** (**m**)	**Kilogram** (**kg**)	**Second** (**S**)	(**N/m2**) **Pascal**

2.1. NUMERICAL MODELLING

2.1.2. Introducing Geometrical Conditions and Specifications of Case Study Materials

In the numerical simulation, to better evaluate and validate the numerical model, it is necessary to compare the results with the valid numerical or laboratory results. Therefore, in the present study, the geometrical and material properties of the studies of Dr. Kianoush and Ghaem Maghami (2010)

were used [9]. The geometrical shape of the tank is shown in Figure 1. As can be seen, in this paper, the flat strain space was used to simulate the tank. Table 2 shows the geometrical conditions and specifications of the materials used in this study.
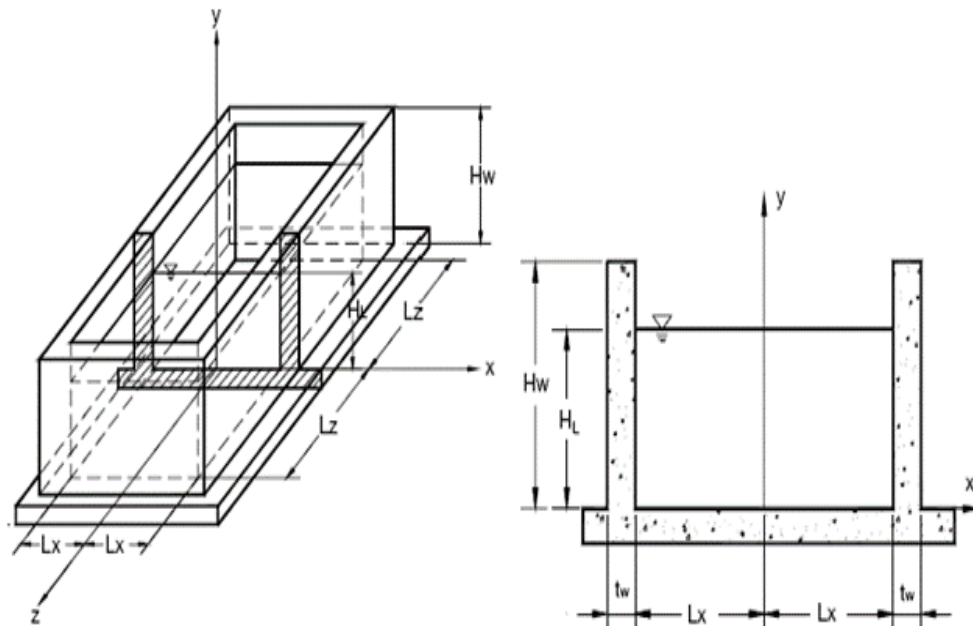
Figure 1. Geometrical conditions of the study tank

Table 2. Materials specifications and geometrical conditions of the tank

Materials specifications			
Concrete density $\rho_c(\text{kg}/\text{m}^3)$	Water density $\rho_l(\text{kg}/\text{m}^3)$	Young's modulus of concrete E(GPa)	Poisson's coefficient of concrete
2300	1000	26.44	0.17
Geometrical conditions of the tank			
(meter) tw	(meter) HL	(meter) Hw	(meter) Lz	(meter) Lx
0.6	5.5	6	30	15

2.1.2. Type of element and how the mesh of the model

In the finite element method, determining the type of element and meshing the model has a significant impact on the convergence of analysis and results [19]. Lagrange elements have been used to simulate the bed environment and concrete tank body. This element is capable of introducing the stress-strain behavior of materials and is suitable for numerical simulation of solid materials. The bed is made for mass simulation. In numerical models where the mass-bed is similar, the energy-absorbing boundary should be used to prevent reflection of seismic waves in far environments. Absorbent element is created by various methods such as dampers, springs, and infinite elements. In this study, the infinite element is used to create an energy absorbent boundary. The finite part has a nonlinear behavior model, and the infinite part has only elastic behavior. Figure 2 illustrates the final meshing pattern of the finite and infinite bed.
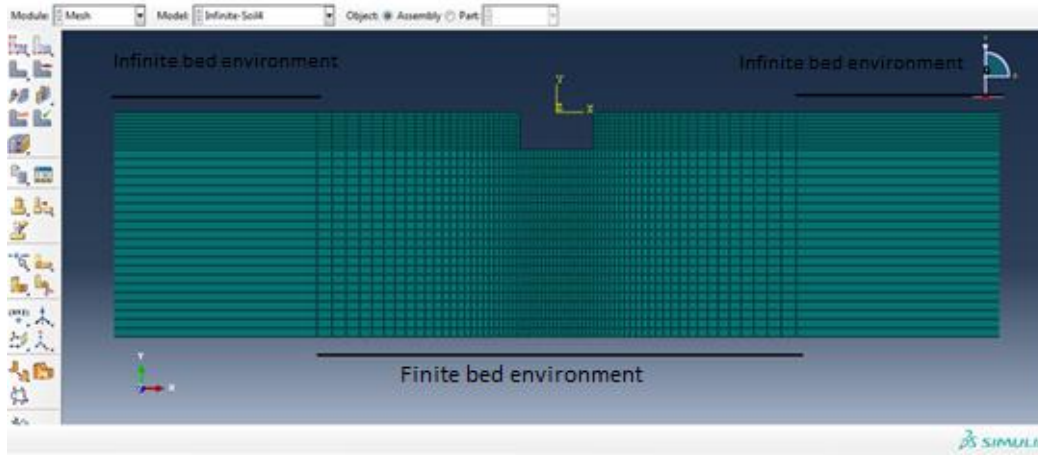
Figure 2. Infinite and finite bed environment
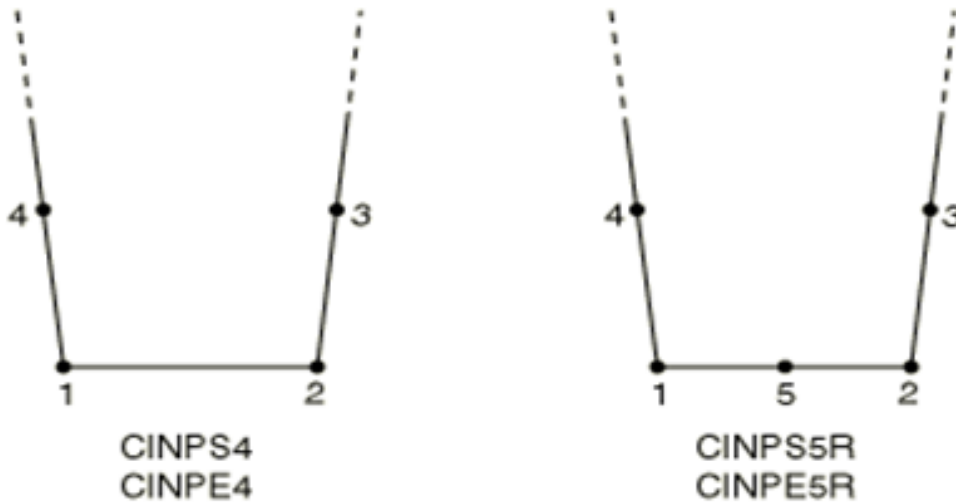

Figure 3. The correct numbering method of the unlimited element in the flat strain and flat stress environment

To simulate the finite part of the bed from the continuous media element an 8-node planar strain with reduced integration form (CPE4R) was used, and to simulate the infinite part from the semi-infinite element a 4-node flat strain with reduced integration formulation (CINPE4) is applied (Figure 3). For modeling the concrete tank body, the joint between the wall and the floor slab of the tank was assumed to be fixed, and the continuous media element of flat strain with reduced integration method (CPE4R) was used. Dimensions and types of elements are obtained based on dimensional analysis of the type and dimension of the element. Figure 4 shows the final meshing of the tank.
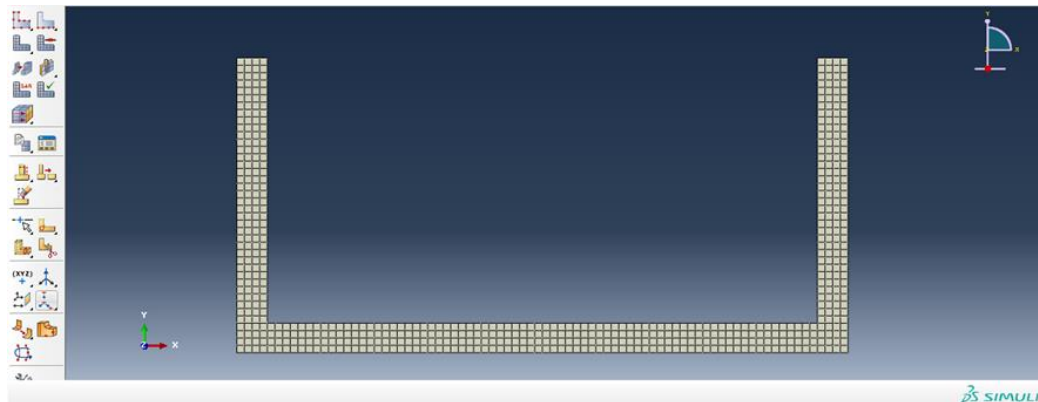

Figure 4. How meshing the tank

For simulating fluid, two methods of adaptive meshing (ALE) and Coupled Eulerian-Lagrangian (CEL) were used.

The reason for using two simulation methods for the fluid environment is to evaluate the validity of the simulation

method of the present study [20, 21]. In the adaptive meshing method, the Hugoniot's Us-Up Linear Theory of the Mie-Gruneisen equation of state is used. Where Us is the shock velocity and Up is the particle velocity which is formulated in the following linear equation:

$$U_s = c_0 + sU_P \quad (1)$$

In this equation, c0 is the sound velocity in a fluid medium, and its value is 1450 m/s. The value of s in this study was zero due to the compactness of fluid medium and the transmission of sound velocity by shock. It should be noted that the Gruneisen constant is considered zero for water. Table 3 shows the parameters of the fluid tank.

Table 3. Water parameters

Density	Dynamic viscosity	Bulk modulus
(kg/m3)	(Ns/m2)	(Gpa)
1000	0.001	2.3

2.1.3. Boundary conditions and gravity loading

In the present numerical model, there are two types of boundary conditions, including lateral and bed floor. The fixed boundary conditions are used for the bed floor, and the infinite element is used as the earthquake energy absorber for the lateral boundary conditions. Gravity loading is applied to the finite bed environment and the concrete tank. In fact, the earth's gravity acceleration was 9.81 m/s2. The software calculated the specific weight of each section using gravity acceleration and volumetric mass and applied to the model. Figure 5 shows the gravity loading. It can be seen that the infinite part will have no gravity loading, and the behavior of this part will be modeled elastically isotropic.
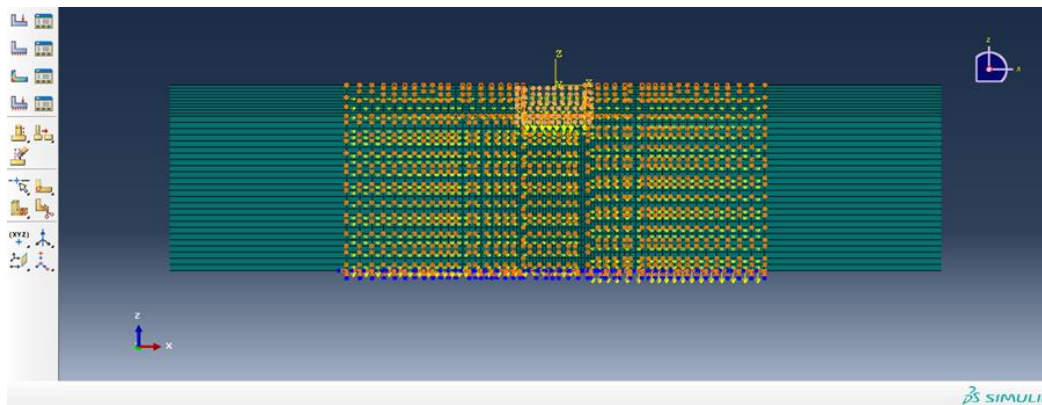

Figure 5. Gravity loading of the numerical model

2.1.4. Introducing interaction

The interaction used in the present study is summarized in Table 4.

Table 4. The introduction of the interaction used in the model

Interaction	Tangential Behavior	Perpendicular behavior	Master level	Slave level
Tank-bed	Without friction	Without influence and separation	Bed	Tank
Tank-fluid	With friction	Without influence	Tank	Fluid

2.1.5. The nonlinear behavioral model of materials

In the present study, an advanced behavioral model of damaged plastic concrete was used to introduce stress-strain behavior of concrete, and to simulate bed behavior, a non-linear behavioral model of Mohr-Coloumb was used. In the present study, for the finite soil, the Mohr-Coloumb behavioral model, along with elastic isotropic behavior was used. In this study, two different rupture mechanisms for

concrete are considered, including tensile rupture and compressive rupture.

2.2. PROBLEM SOLVING METHOD

The explicit dynamic method is used to solve the modeling of this research.

2.2.1. Introducing earthquake records used in research

The near-fault range is usually assumed to be within the range of 10 to 60 km from the active fault. In this range, earthquakes usually depend on the rupture mechanism, direction of rupture propagation relative to the site, and permanent displacement due to faulting. Therefore, the accelerograms in the range of less than 10 km and more than 60 km were used for selection of near and far fault accelerograms. It should be noted that due to the significant effects of vertical earthquake acceleration in near-fault earthquakes, earthquake acceleration has also been applied in a vertical direction. Therefore, for more accurate estimation, the pair of near and far-field accelerograms have been used for identical seismic excitations.In 1999, 7.4 magnitude earthquake occurred in Kocaeli, the northern region of Turkey.
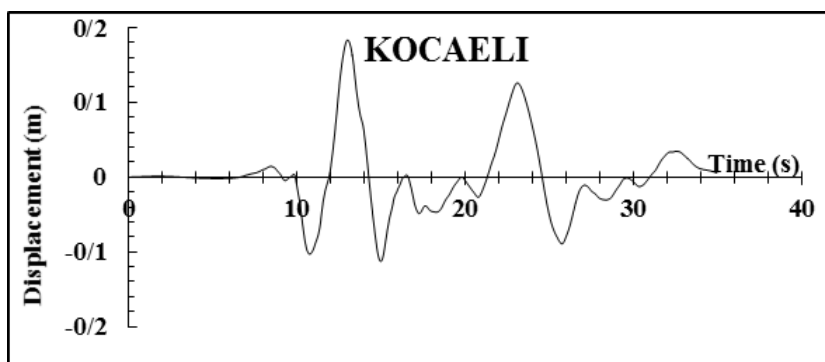

Figure 6. Kocaeli earthquake displacement spectrum

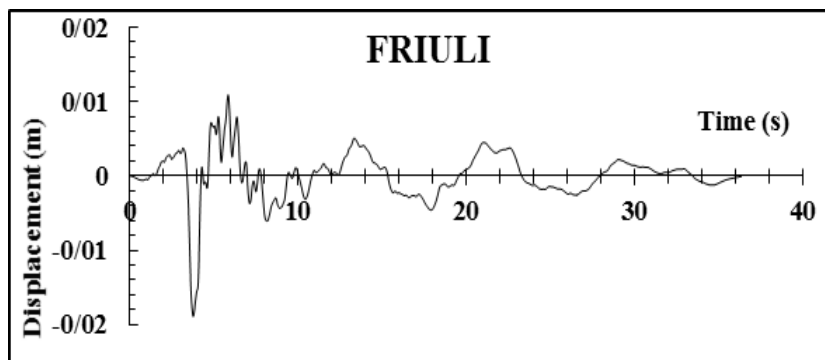The FRIULI earthquake occurred in 1976 in the northern part of Italy.

Figure 7. FRIULI earthquake displacement spectrum

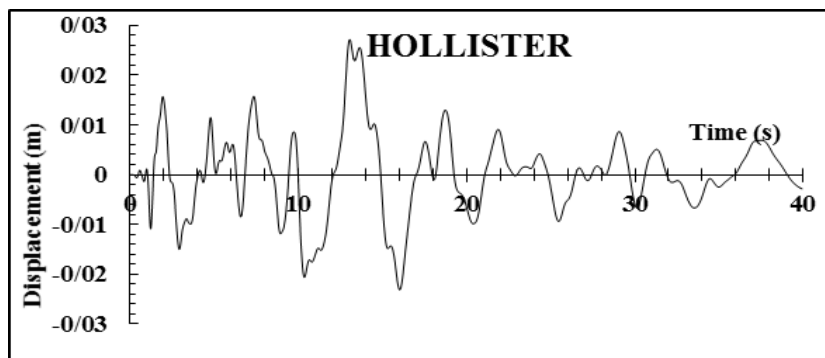HOLLISTER earthquake occurred in 1989 in San Francisco with a magnitude of 6.8.

Figure 8. HOLLISTER earthquake displacement spectrum

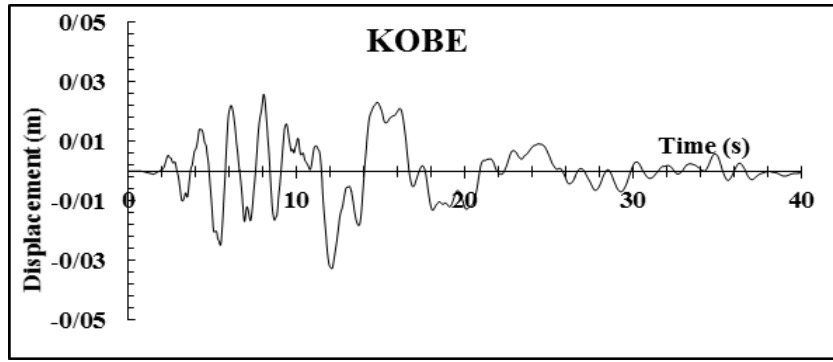In June 1995, the KOBE earthquake with a magnitude of 6.8 occurred 20 km from Kobe city in Japan.

Figure 9. KOBE earthquake displacement spectrum

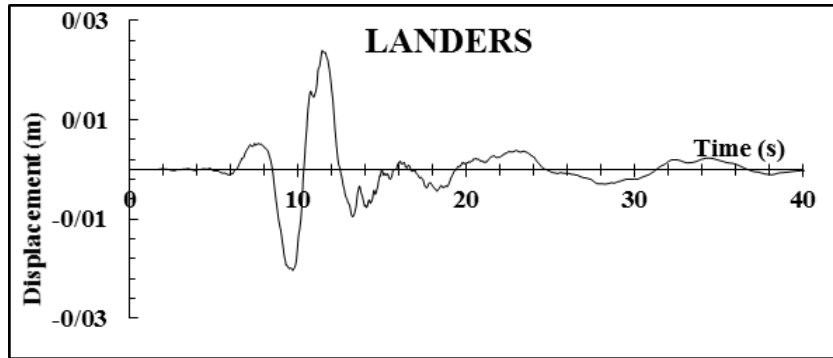The LANDERS earthquake occurred in 1992 in the city of Landers, California.

Figure 10. LANDERS earthquake displacement spectrum

The Imperial Valley earthquake occurred in 1979 in the southern part of Mexico City with a magnitude of 6.4.
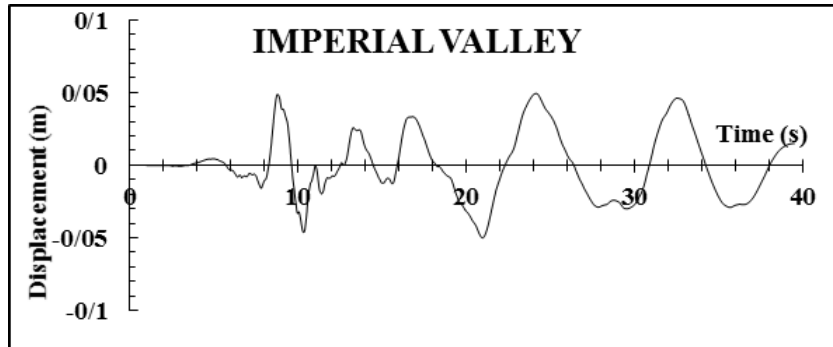

Figure 11. IMPERIALVALLEY earthquake displacement spectrum

The Chi-Chi earthquake occurred in September 1999 in Poli, Taiwan, due to the opening and rapture of the Chelungpu fault. The magnitude of the earthquake was 7.5 Richter. Four aftershocks also occurred with a magnitude of more than 6.5 Richter.
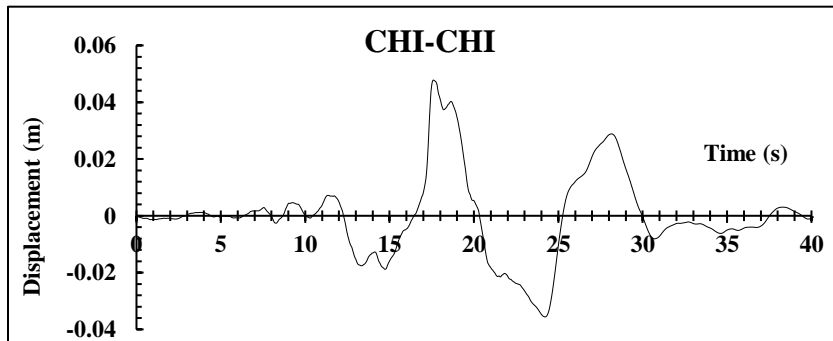

Figure 12. CHICHI earthquake displacement spectrum

NORTHRIDGE earthquake occurred in June 1994, 30 kilometers north of Los Angeles, in Northridge. The

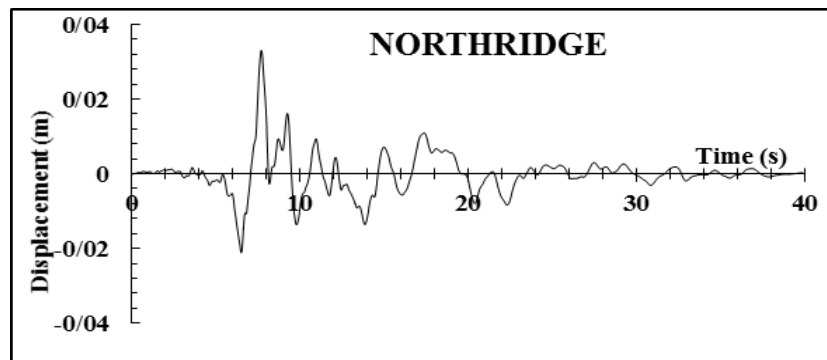magnitude of the earthquake was 6.9 Richter, with a peak acceleration of 0.5g and 19 km deep-focus.

Figure 13. NORTHRIDGE earthquake displacement spectrum

In September 1979, the 7.8 magnitude Tabas

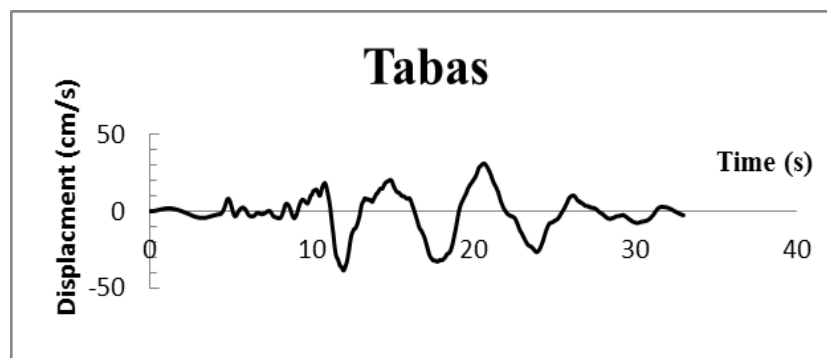earthquake destroyed Tabas and its adjacent villages.

Figure 14. Tabas earthquake displacement spectrum

Bam earthquake with a magnitude of 6.6 Richter

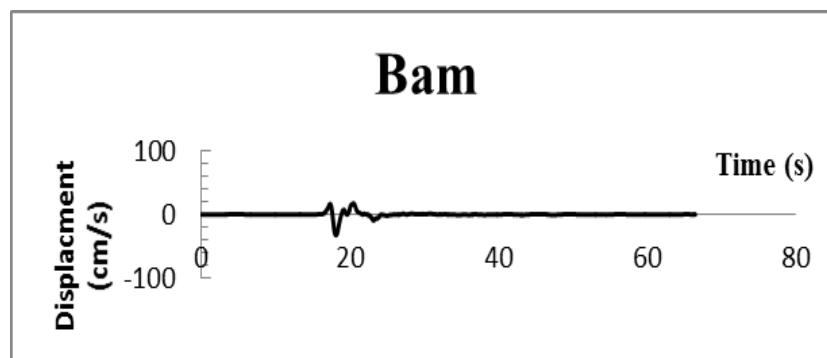occurred in 2003 in the city of Bam in Kerman province.

Figure 15. Bam earthquake displacement spectrum

2.3. MODEL VALIDATION

Various analyzes should be performed to ensure the accuracy of the numerical model results. In modeling associated with soil-structure interaction, boundary distance convergence analysis should be performed. The boundary distances analyzed in this study are shown in Figure 16. Thus, the dependence of the modeling results on these boundary distances was evaluated. According to the technical literature, the boundary distance of the infinite bed was considered half of the total length of the finite bed. Infinite lengths were therefore determined and controlled

for each selection from the finite bed. Therefore, for the other two boundary distances, sensitivity analysis of boundary distance was performed. The results of this analysis for the optimal boundary distances are presented in Table 5. According to this table, the most suitable lateral boundary distance of finite bed, infinite boundary distance, and finite floor bed boundary distance were obtained 80 m, 80 m, and 100 m, respectively.
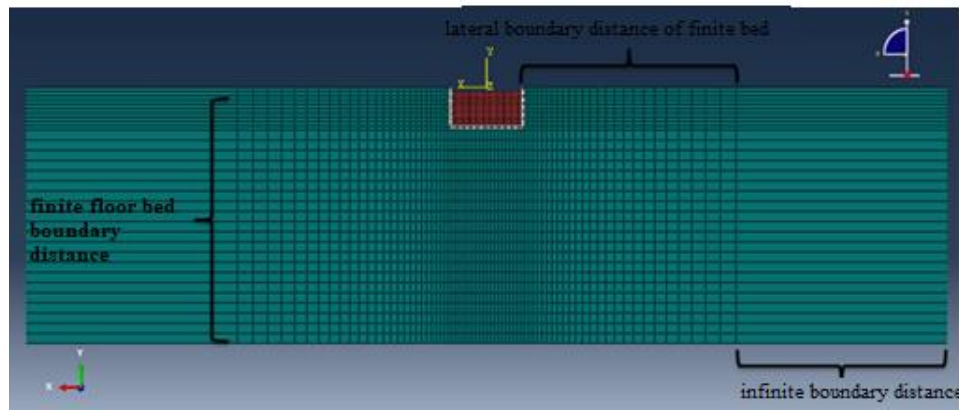
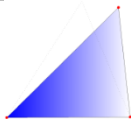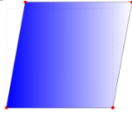**Figure 16.** Boundary distances investigated in the sensitivity analysis

Table 5. Boundary distance values determined based on sensitivity analysis

Boundary distance	Unit	Displacement	Stress	Optimal boundary distance
Lateral bed	(**meter**)	80	70	80
Floor bed	(**meter**)	90	100	100
Infinite bed	(**meter**)	80 meters (half the total length of the finite media)		

In addition to boundary distance analysis, the type and dimensions of the element used in the component analysis will have a significant effect on the results. Accordingly, the optimal type and length of the element used were determined using element type sensitivity analysis and element dimension sensitivity analysis. The plain strain with dimensions of 7.5, 10, 12.5, 15, and 17.5 cm was investigated to analyze the sensitivity of the type and dimensions of the four and three nodal elements. Table 6 shows the type, length, and number of elements used in the sensitivity analysis.

Table 6. Type, length, and number of elements and time of sensitivity analysis

| Three-node plain strain element with full integration form		CPE3	Four-node plain strain element with reduced integration form		CPE4R
Approximate size (cm)	7.5	Analysis time	Approximate size (cm)	7.5	Analysis time
		5230			4140
Approximate size (cm)	10	Analysis time	Approximate size (cm)	10	Analysis time
		4760			3450
Approximate size (cm)	12.5	Analysis time	Approximate size (cm)	12.5	Analysis time
		3330			2630
Approximate size (cm)	15	Analysis time	Approximate size (cm)	15	Analysis time
		2710			1920
Approximate size (cm)	17.5	Analysis time	Approximate size (cm)	17.5	Analysis time
		1980			1448
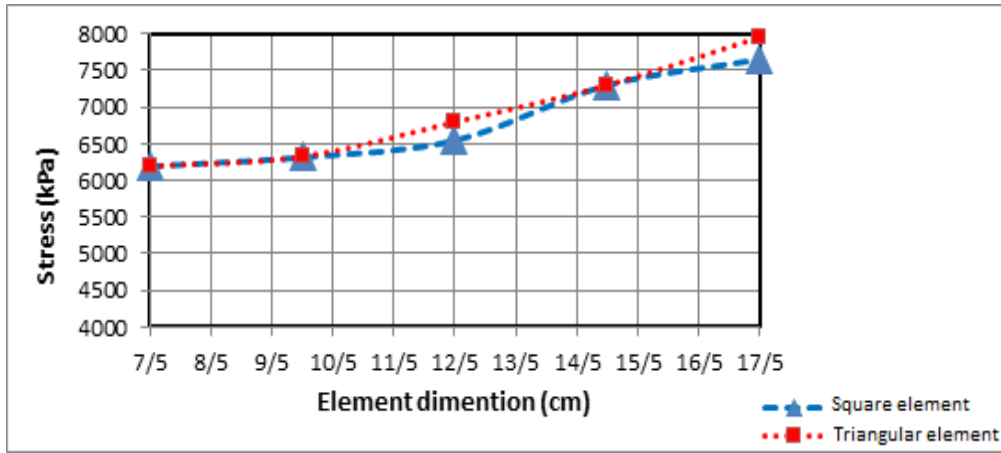
Figure 17. Results of element sensitivity analysis
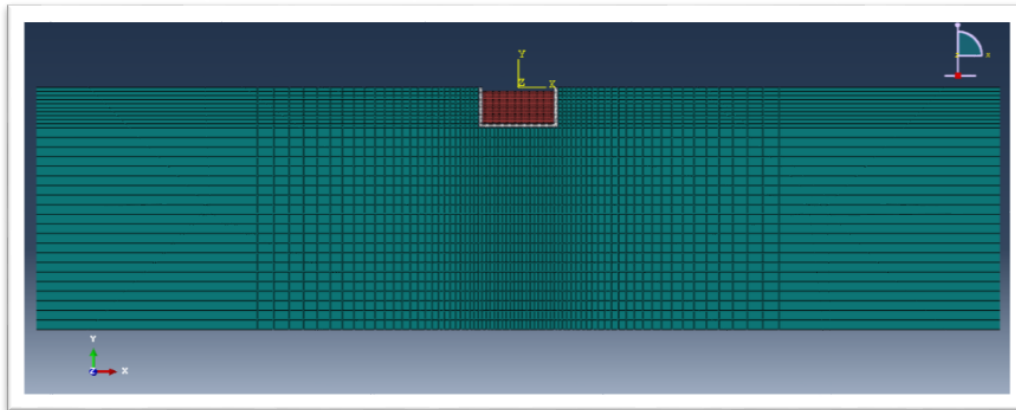
Figure 18. Optimal meshing pattern

After sensitivity analysis of boundary distance and element sensitivity analysis, the results were compared with a numerical model of valid papers and references. For this purpose, the numerical model of Kianoush and Ghaem Maghami [9] was evaluated. For this purpose, the geometry and meshing of the numerical model are presented in Figure 19. It should be noted that for this model, the adaptive mesh

method is used to simulate the fluid. The comparison of the results of the sloshing time history of the free surface of the fluid reservoir is shown in Figure 20. The results are consistent with the outputs of the Elsentro accelerogram. Thus, the graph's ups and downs were similar, with a maximum difference of less than 8%.
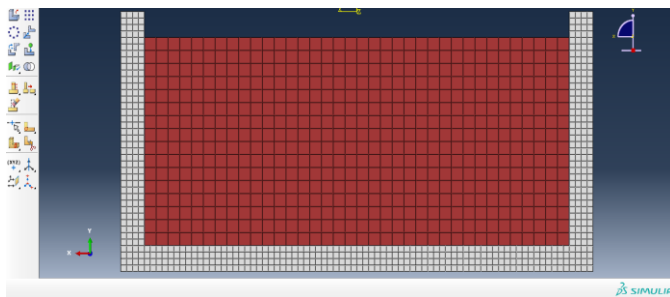
B) numerical model by the present research method
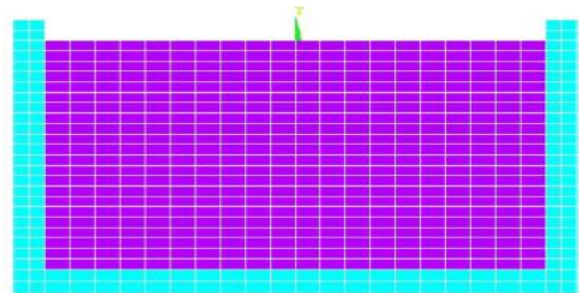
A) The numerical model of Kianoush et al

Figure 19. Comparison of the geometrical conditions of the validation model with the model of Kianoush et al. [9]

| B) Time history of the reservoir free surface of the present model | A) Time history of the reservoir free surface of Kianoush model |

Figure 20. Comparison of sloshing history of free fluid reservoir validation model with Kianoush model. [9]

2.4. INTRUDUCING NUMERICAL SAMPLES AND RESEARCH METHODS

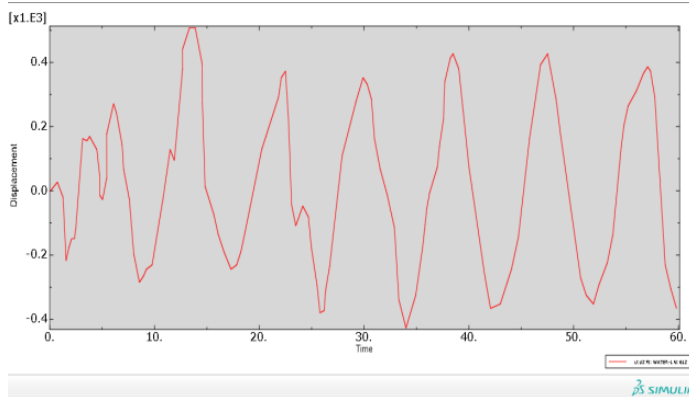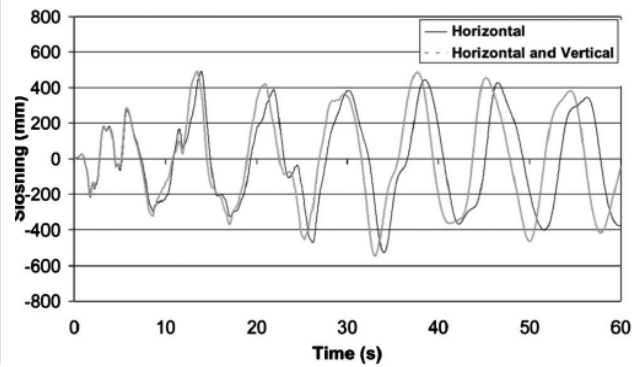In the present study, to accurately evaluate the seismic performance of the reservoir, the analytical-statistical method of the fragility curve is used. For this purpose, the reservoir-fluid-bed system was simulated with advanced assumptions, and its results were used for statistical analyses using the failure curve.

3. RESULTS AND DISCUSSION

3.1. FRAGLITY CURVES

In the present study, the soil-structure-fluid model of the concrete reservoir was analyzed using the finite element method for 200 real and scaled accelerograms with 0.125 g steps. The failure index for each accelerogram was determined based on the earthquake intensity parameter. The data obtained from numerical analysis were analyzed using Easyfit software. The probability density function and the fragility curve were obtained for different failure levels. In this section, data obtained from numerical analysis of Abaqus software and statistical analysis results with Easyfit software are presented for fragility curves: low failure under far and near field accelerogram and severe damage under far and near field accelerogram. The following table shows the data obtained from the numerical analysis of the soil-structure-fluid interaction system for low failure index under far-field accelerograms. It should be noted that the scaled steps are considered with a range of 0.125 g. If the low failure index occurs for numbers between time steps, the upstream and downstream failure value is determined by interpolating the maximum values. The probability density function (data frequency) and the functions of the normal distribution, log-normal distribution, and gamma distribution for this failure index are shown in Figure 21. As can be seen, the log-normal is the most appropriate distribution function. Therefore, this distribution function is used to analyze the failure curve. Figures 22 and 23 show the log-normal function and the fragility curve of the concrete tank system under soil-structure-fluid interaction for the low failure index under the far-fault accelerograms, respectively. The results show that the maximum acceleration amplitude for low failure under far fault excitation is 0 to about 0.625 g. 10% failure probability is obtained For PGA = 0.15g. 30% failure probability is reported for the maximum acceleration of less than 0.2 g. In fact, by increasing 0.1 for maximum acceleration, the probability of failure is increased by 20%. A 90% failure probability is obtained for PGA= 0.52g. Eventually, at a maximum acceleration of 0.6 g, the low failure will occur for far-fault excitations, and this reservoir will be damaged for the accelerograms with a maximum value of 0.6 g.

Table 7. Determining the PGA of low failure for far-field accelerograms

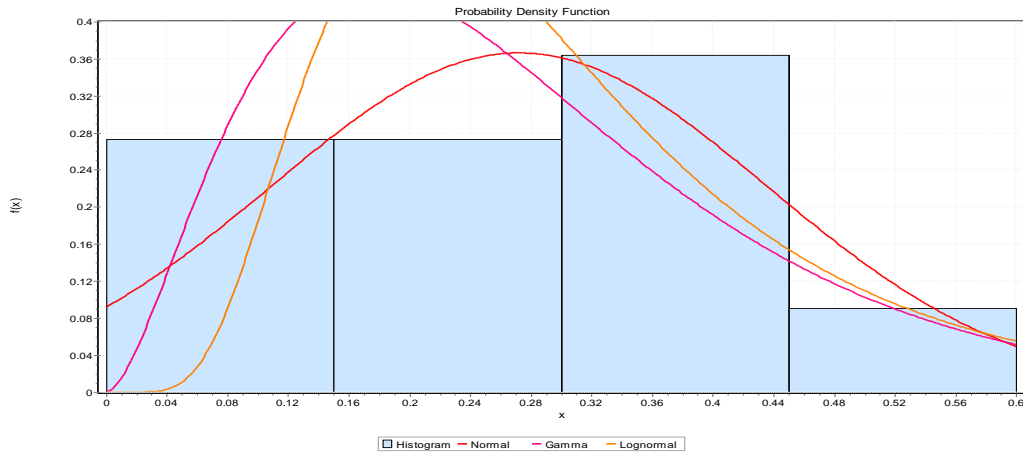|	0.125g	0.25g	0.375g	0.5g	0.625g
Northridge	0.126	-	-	-	-
Tabas		0.27	-	-	-
Hollster	0.1	-	-	-	-
Imperial valley	-	-	0.41		-
Kobe		0.22	-	-	-
Bam	-		0.35	-	-
CHI-CHI	-		0.32	-	-
Landers	-	0.25	-	-	-
Friuli	-		0.36	-	-
Kocaeli	-	-	-	0.605	

Figure 21. Probability density function and functions of the normal distribution, log normal, and gamma distribution for low failure index under far-field accelerograms
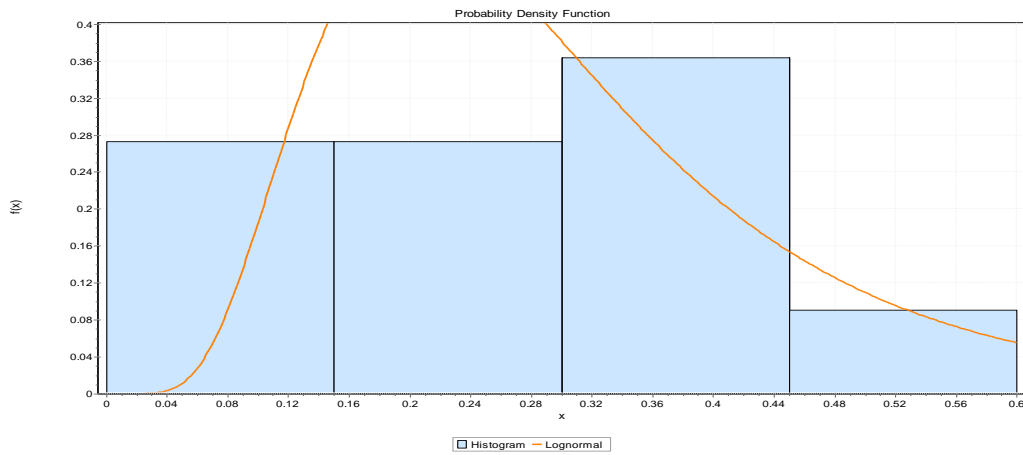

Figure 22. Log normal distribution function for low failure index under far-field accelerograms

Figure 23. Fragility curve for low failure index under far-field accelerograms

Table 8 shows the results of the numerical simulation of the soil-structure-fluid interaction system for the severe failure index under far-field accelerograms. Figures 24 and 25 show the results of the probability density function and functions of the normal distribution, log normal distribution, and gamma distribution. Analysis of the fragility curve for far-field accelerograms in Easyfit software (Figure 26) indicates that severe failure will occur

for the maximum gravity acceleration range of 0.45 to 1.25. The failure probability of maximum acceleration was reported 10 and 20% for 0.63 and 0.7 g, respectively, and 30% for PGA = 0.76. The probability of severe failure of the concrete tank for the peak of 0.9 g is about 60%, and by increasing this peak up to 1.1 g, the probability reaches 90%. The results show that for the maximum acceleration of more than 1.25 g, the probability of severe failure for this

reservoir will be definite, and the reservoir will collapse. Previous studies [22, 23] have also shown that this acceleration will lead to such a result. The probability of severe failure of the concrete tank understudy for the maximum 0.9 g is about 60%, and by increasing this limit to 1.1 g, the probability is 90%. The results show that for the maximum acceleration of more than 1.25 g, the probability of severe failure for this reservoir will be definite, and the reservoir will collapse. That would be the result.

Table 8. Determining the PGA of low failure for far-field accelerograms

	0.125g	0.25g	0.375g	0.5g	0.625g	0.75g	0.875g	1g	1.125g	1.5g
Northridge	-	-	-	-	**0.624**	-	-	-	-	-
Friuli	-	-	-	-	-	**0.76**	-	-	-	-
Tabas	-	-	-	**0.58**	-	-	-	-	-	-
Imperial valley	-	-	-	-	-	-	-	-	1.13	
Kobe	-	-	-	-	-	**0.72**	-	-	-	-
Bam	-	-	-	-	-	-	**0.945**	-	-	-
CHI-CHI	-	-	-	-	-	-	-	**0.89**	-	-
Landers	-	-	-	-	-	-	**0.83**	-	-	-
Hollster	-	-	-	-	-	-	-	-		1.22
Kocaeli	-	-	-	-	-	-	-	-	**1.25**	-

Figure 24. Probability density function and functions of the normal distribution, log normal, and gamma distribution for low failure index under far-field accelerograms

Figure 25. Log normal distribution function for low failure index under far-field accelerograms
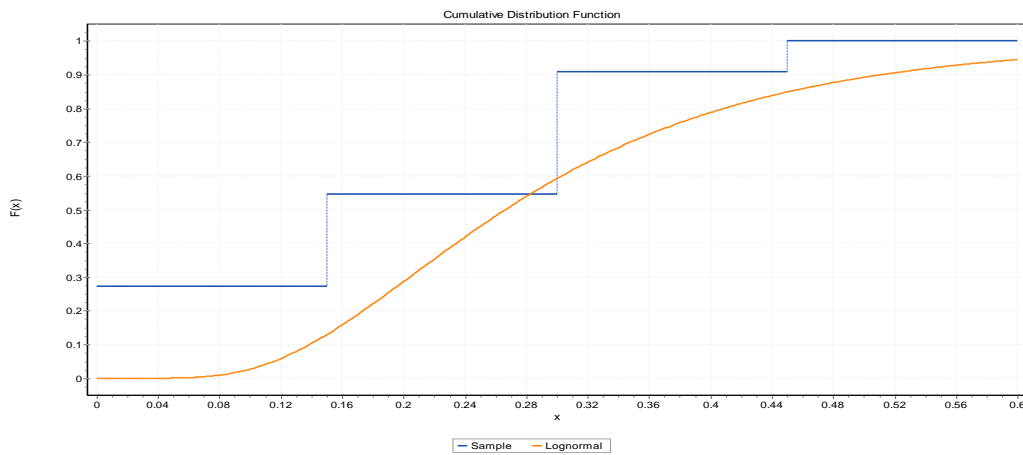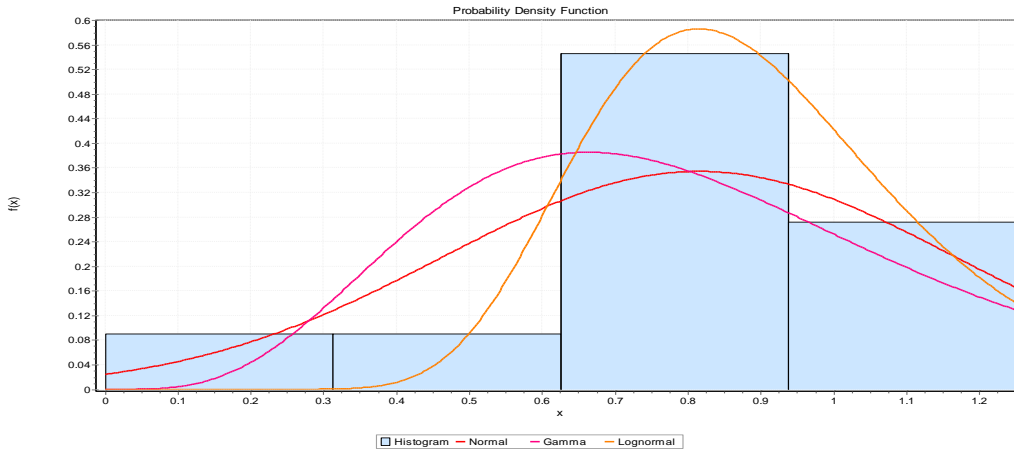
Figure 26. Fragility curve for low failure index under far-field accelerograms

The maximum acceleration values for the numerical samples under near-fault excitations with a low failure index are presented in Table 9. In these conditions, according to Figures 27 and 28, the best function is log-normal distribution. The fragility curve obtained from this distribution function in Figure 29 shows that the range of low failure in the near-fault field would be 0.045 to 0.3

gravity acceleration. So the maximum acceleration of 0.08 and 0.09 indicate a 10 and 20% failure probability. 60% and 90% failure probability were reported at the peak of 0.15 g and PGA = 0.23g, respectively. The low failure will occur for near-field accelerograms with a maximum acceleration of more than 0.3 g.

Table 9. Determining the PGA of low failure for far-field accelerograms

	0.125g	0.25g	0.375g	0.5g	0.625g	0.75g	0.875g	1g	1.125g	1.5g
Northridge	0.08	-	-	-	-	-	-	-	-	-
Tabas	0.1	-	-	-	-	-	-	-	-	-
Hollster	0.07	-	-	-	-	-	-	-	-	-
Imperial valley	-		0.3	-	-	-	-	-	-	-
Kobe		1.4	-	-	-	-	-	-	-	-
Bam		1.35	-	-	-	-	-	-	-	-
CHI-CHI		1.55	-	-	-	-	-	-	-	-
Landers	0.11	-	-	-	-	-	-	-	-	-
Friuli		1.8	-	-	-	-	-	-	-	-
Kocaeli		0.2	-	-	-	-	-	-	-	
										-

Figure 27. Probability density function and functions of the normal distribution, log normal, and gamma distribution for low failure index under far-field accelerograms
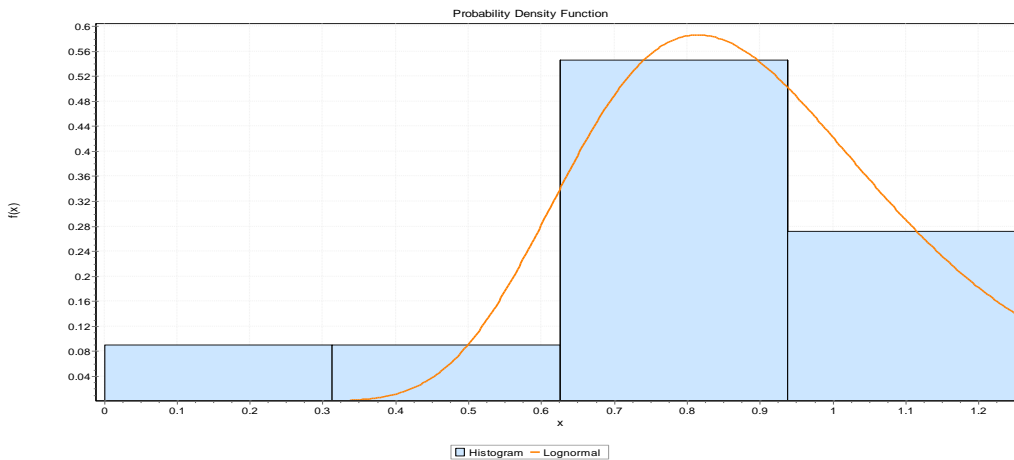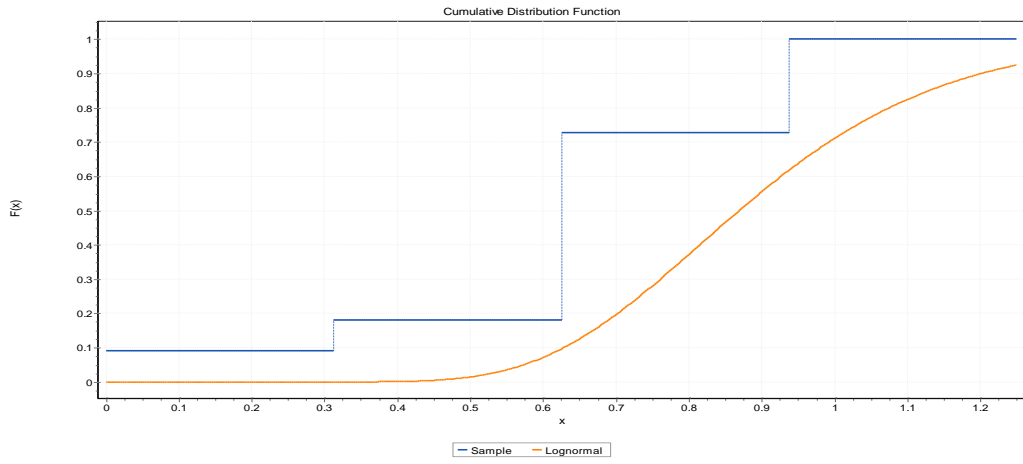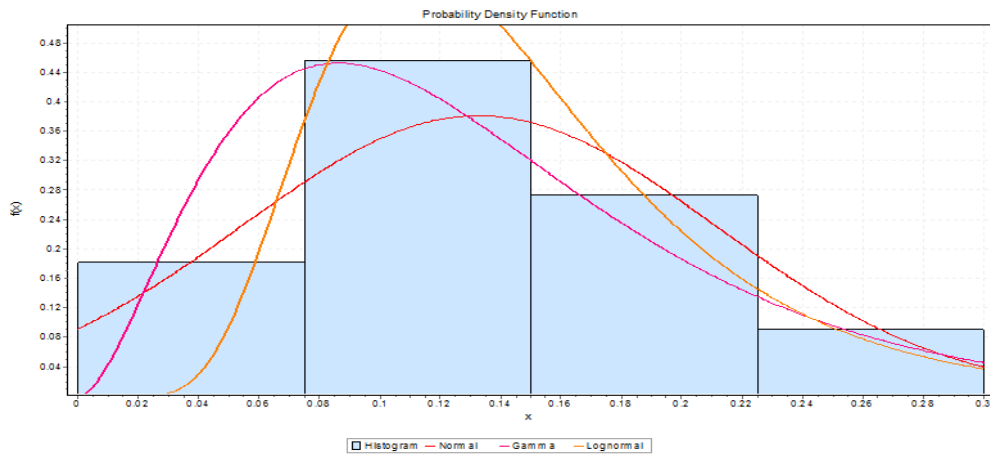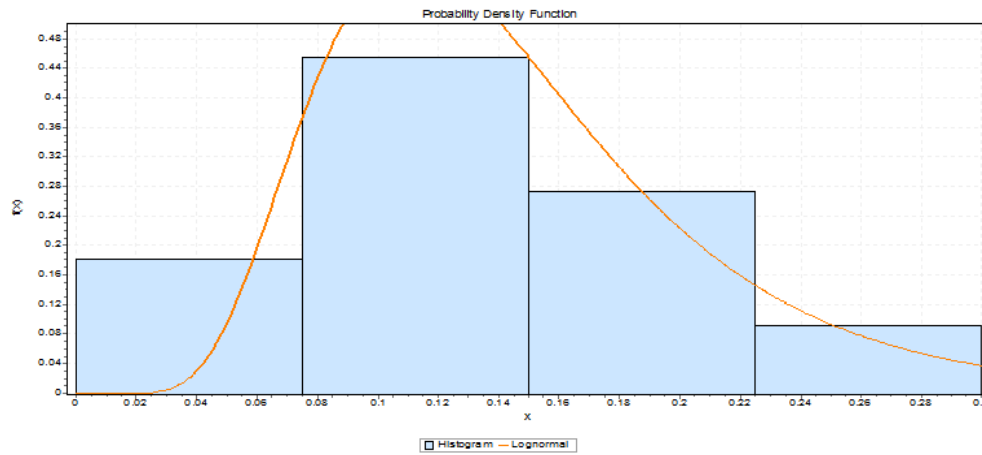
Figure 28. Log normal distribution function for low failure index under far-field accelerograms
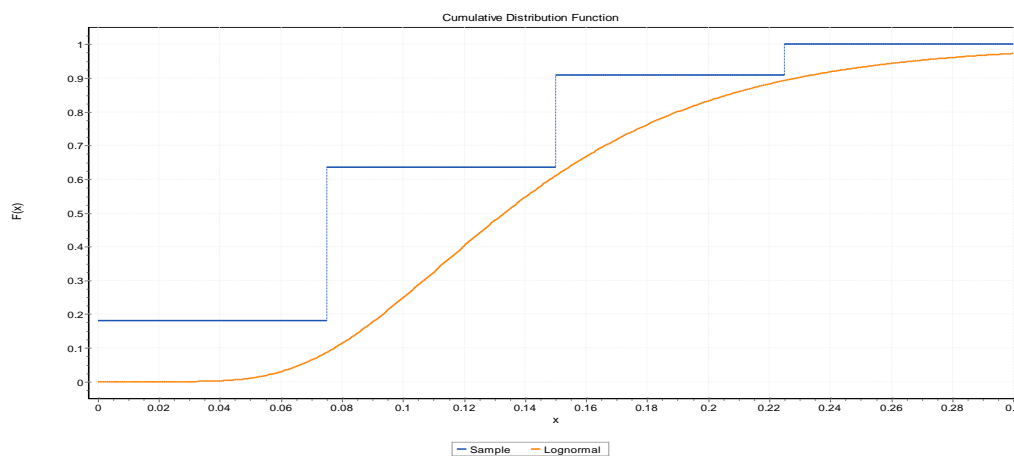

Figure 29. Fragility curve for low failure index under far-field accelerograms

Table 10 shows the results of the numerical simulation of the reservoir-reservoir-foundation interaction system for the severe failure index under near-field accelerograms. Figures 30 and 31 show the results of the probability density function and the functions of the normal distribution, the log normal distribution, and the gamma distribution. It can be seen that the most appropriate distribution function is log-normal. So, this distribution function is used to analyze the fragility curve. According to the fragility curve obtained in

Easyfit software (Figure 32), it is observed that for the maximum acceleration of 0.55 g to 0.6 g, the probability of failure is 10 and 20%, respectively, and the 30% failure rate is determined at PGA = 0.6g. The maximum acceleration of 0.75 g for the severe failure level is 60%, and only by reaching PGA = 0.8g the probability of failure increase by 90%. For maximum acceleration more than 1/1 gravity acceleration, severe failure occurs in this tank.

Table 10. Determining the PGA of low failure for near-field accelerograms

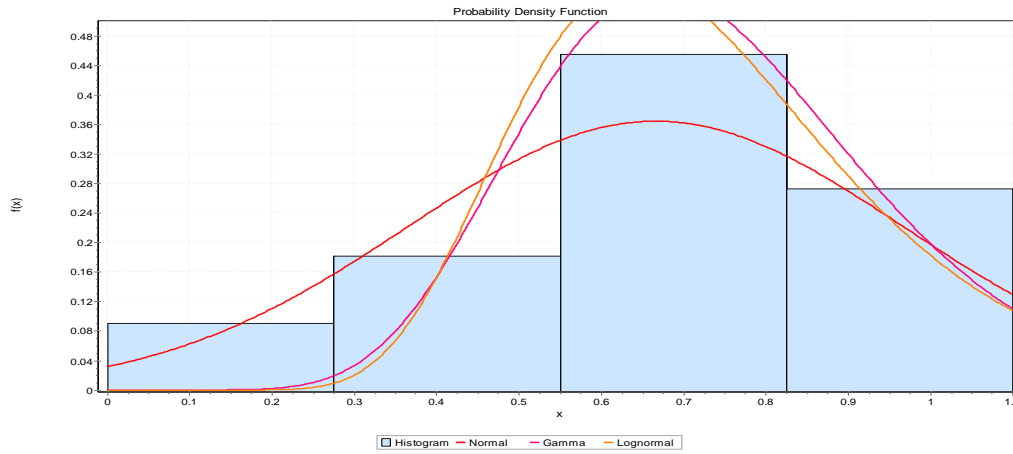|	0.125g	0.25g	0.375g	0.5g	0.625g	0.75g	0.875g	1g	1.125g	1.5g
Northridge	-	-	-	0.55		-	-	-	-	-
Tabas	-	-	-	0.6		-	-	-	-	-
Hollster	-	-	-	0.5	-	-	-	-	-	-
Imperial valley	-	-	-	-	-	-	0.81	-	-	-
Kobe	-	-	-	-	-	0.75	-	-	-	-
Bam	-	-	-	-	-	0.79		-	-	-
CHI-CHI	-	-	-	-	-	-	0.88	-	-	-
Landers	-	-	0.41	-	-	-	-	-	-	-
Friuli	-	-	-	-	-	-	0.94	-	-	-
Kocaeli	-	-	-	-	-	-	-	-	1.1	-

Figure 30. Probability density function and functions of the normal distribution, log normal, and gamma distribution for low failure index under near-field accelerograms
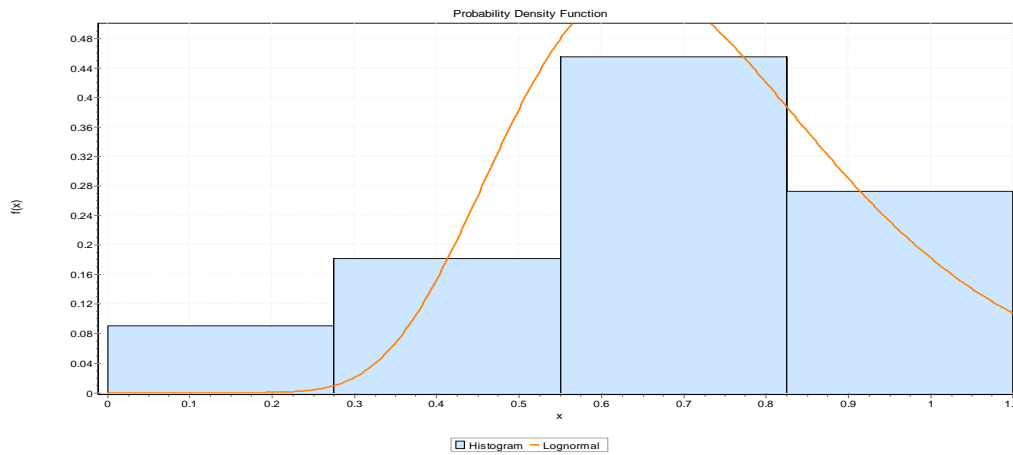

Figure 31. Log normal distribution function for low failure index under near-field accelerograms
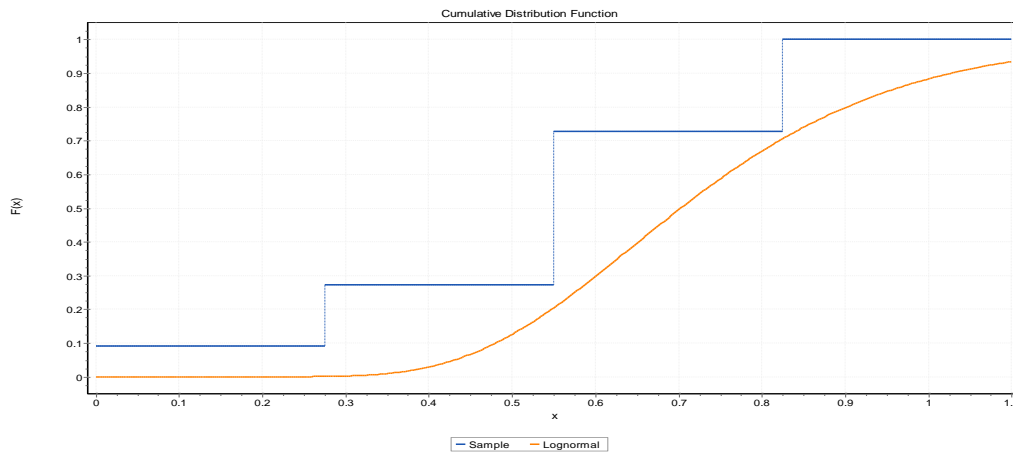

Figure 32. Fragility curve for low failure index under near-field accelerograms

To comparing the results, all the fragility curves are plotted in Figure 33. Comparison of the fragility curves shows that the probability of a low failure for the near-field accelerograms occurs at the less maximum acceleration than the far-field and is plotted as S. This means that the dispersion of maximum acceleration in the near-field excitations is less than similar far-field excitations. The results for the low failure index show that for maximum

earthquake acceleration more than 0.3 g, the reservoir structure will be damaged under near-fault excitation. However, for similar far-field excitations, this failure has been reported for maximum acceleration more than 0.6 g. Therefore, due to the frequency contents and pulse effects and vertical earthquake acceleration in near-field excitations, a low failure at less maximum acceleration has occurred. So that for low failure f (t) = 1 the maximum value

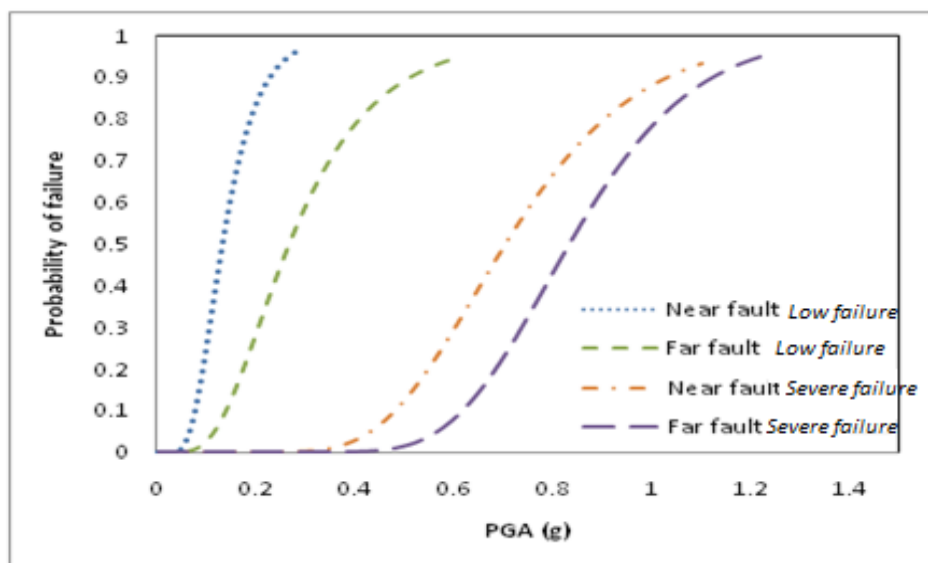of near-field acceleration is half of the maximum near-field acceleration.

Figure 33. Comparison of far and near field curves with low and severe failure index

For severe failure, critical conditions are obtained for the near field. So that for similar failure probability, severe failure in the far-fault state is obtained at more maximum accelerations. In severe failure for two diagrams of far and near-fault the graph is as horizontal S. Therefore, a wider PAG amplitude is obtained so that for near field conditions this maximum acceleration range is from 0.4 to 1.1 gravity acceleration and for far-field conditions, the range of maximum acceleration is from 0.55 g to 1.25 g. For the concrete tank understudy, the probability of severe failure will most definitely occur for near-field excitations at the maximum acceleration of 1 g, while this failure occurs for far-field excitations at 1.25 g.

4. CONCLUSION

- The proposed modeling method of the present study is accurate enough to simulate the reservoir-bed-fluid interaction system and can be used for seismic parametric studies.

- To obtain accurate numerical results in problems with mass bed simulation, boundary distance convergence analysis for lateral boundaries, bed boundary is of particular importance. The results cannot be assured if the boundaries are inappropriate.

- The dynamic explicit method is a suitable tool for analyzing dynamic problems of soil-structure-fluid interaction. This method has a simplifying assumption for analyzing problems in which determining the appropriate stability time is of particular importance. In case of failure to choose the right time of stability, the analysis will diverge. The stability time is directly related to the smallest dimension of the element and is inversely related to the shear wave velocity of the materials. Therefore, special attention should be paid to the convergence analysis of dimension and type of the element.

- The results show that the log normal function is the most appropriate distribution function for all the fragility curves, and this distribution function is used to analyze the fragility curve.

- The results show that the maximum acceleration amplitude for low failure probability under far-fault excitations is in a range of 0 to 0.6 g. For PGA = 0.15g a 10% failure probability is obtained and 30% failure probability is reported for the maximum acceleration of less than 0.2 g. In fact, by increasing only 0.1 of maximum acceleration, the failure probability is increased by 20%.

- For the maximum acceleration of 0.3 g3, a 60% probability of failure is recorded, and a 30% increase is obtained for a maximum of 0.2 to 0.3 gravity acceleration. A 90% probability of failure is obtained for PGA = 0.52g, and eventually, at a maximum of 0.6 g, low failure occurs for far-field excitation, and the low failure occurs in this reservoir for the accelerograms with a maximum of 0.6 g.

- Severe failure will occur for the maximum acceleration range of 0.45 to 1.25 gravity acceleration. Failure probability for the maximum accelerations of 0.63 and 0.7 g is reported 10 and 20%, respectively, and 30% for PGA = 0.76.

- The severe failure probability of the concrete tank is determined by about 60% for a maximum of 0.9 g, and by increasing this maximum up to 1.1 g, the failure probability increases by 90%. The results show that for maximum acceleration more than 1.25 g, the probability of severe failure is definite for this tank.

···

- The low failure range in the near-fault field will be 0.04 to 0.3 gravity acceleration. So that the maximum acceleration of 0.08 and 0.09 indicate a 10% and 20% failure probability. A 0.15 g maximum indicates a 60% probability of failure, and a 90% probability of failure is reported at PGA = 0.23g. The low failure will occur in this reservoir for near-field accelerograms with a maximum acceleration of more than 0.3g.

- For a maximum acceleration of 0.5 g to 0.6 g, the probability of failure is 10% and 20%, and a 30% probability of failure is determined at PGA = 0.6g. The maximum acceleration of 0.75 g for the severe failure level is 60%, and only at PGA = 0.8g the probability of failure increase by 90%. For maximum acceleration more than 1/1 gravity acceleration, severe failure occurs in this tank.

- Comparison of fragility curves shows that the low failure probability for near-field accelerograms occurs at the less maximum acceleration compared to the far-field accelerograms and is plotted as perpendicular S. This means that the dispersion of maximum accelerograms in the near-field excitations is less than in the far-field excitations. The results for the low failure index show that for maximum earthquake acceleration more than 0.3 g, the failure will occur in reservoir structure under near-fault excitations, whereas for similar far-field excitations, this failure is reported for maximum accelerations more than 0.6 g. Therefore, due to the frequency contents and pulse effects and vertical earthquake acceleration in near-field excitations, a low failure has occurred at less maximum acceleration. So that for low failure f (t) = 1 the maximum value of near-field acceleration is half of the maximum near-field acceleration.

- For severe failure, critical conditions are reported for the near- field. So that for similar failure probability, severe failure is achieved in far-fault state at more maximum accelerations. In severe failure mode for two near and far fault diagrams, the graph is as vertical S. Therefore, the wider PAG amplitude is obtained. So that the maximum acceleration amplitude for near-field conditions is from 0.4 to 1.1 gravity acceleration and for far-field conditions is from 0.55 g to 1.25 g. For the concrete tank understudy, the probability of severe failure will most definitely occur for near-field excitations from the maximum acceleration of 1 g, while this failure occurs for far-field excitations from the maximum acceleration of 1.25 g.

5. REFERENCES

[1] Leão S, Roux P, Loiseau E, Junqua G, Sferratore A, Penru Y, Rosenbaum RK. Prospective Water Supply Mix for Life Cycle Assessment and Resource Policy Support—Assessment of Forecasting Scenarios Accounting for Future Changes in Water Demand and Availability. Environmental science & technology. 2019 Jan 10;53(3):1374-84. [View at Google Scholar] ; [View at Publisher].

[2] Naseri F, Bagherzadehkhalkhali A. Investigation into the effect of bed stiffness on seismic performance of concrete gravity dam under far-and near-field earthquakes. Journal of civil Engineering and Materials Application. 2019 Mar 1;3(1):40-52. [View at Google Scholar] ; [View at Publisher].

[3] Mata J. Interpretation of concrete dam behaviour with artificial neural network and multiple linear regression models. Engineering Structures. 2011 Mar 1;33(3):903-10. [View at Google Scholar] ; [View at Publisher].

[4] Dai B, Gu C, Zhao E, Zhu K, Cao W, Qin X. Improved online sequential extreme learning machine for identifying crack behavior in concrete dam. Advances in Structural Engineering. 2019 Jan;22(2):402-12. [View at Google Scholar] ; [View at Publisher].

[5] Shariatmadari N, Lasaki BA, Eshghinezhad H, Alidoust P. Effects of landfill leachate on mechanical behaviour of adjacent soil: A case study of saravan landfill, rasht, iran. International Journal of Civil Engineering. 2018 Oct 1;16(10):1503-13.[View at Google Scholar] ; [View at Publisher].

[6] Fang HW, Rodi W. Three-dimensional calculations of flow and suspended sediment transport in the neighborhood of the dam for the Three Gorges Project (TGP) reservoir in the Yangtze River. Journal of Hydraulic Research. 2003 Jul 1;41(4):379-94. [View at Google Scholar] ; [View at Publisher].

[7] Housner GW. Dynamic pressures on accelerated fluid containers. Bulletin of the seismological society of America. 1957 Jan 1;47(1):15-35. [View at Google Scholar] ; [View at Publisher].

[8] Kianoush MR, Chen JZ. Effect of vertical acceleration on response of concrete rectangular liquid storage tanks. Engineering structures. 2006 Apr 1;28(5):704-15. [View at Google Scholar] ; [View at Publisher].

[9] Kianoush MR, Ghaemmaghami AR. The effect of earthquake frequency content on the seismic behavior of concrete rectangular liquid tanks using the finite element method incorporating soil–structure interaction. Engineering Structures. 2011 Jul 1;33(7):2186-200. [View at Google Scholar] ; [View at Publisher].

[10] Eshghi S, Razzaghi MS. Performance of industrial facilities in the 2003 Bam, Iran, earthquake. Earthquake Spectra. 2005 Dec;21(S1):395-410. [View at Google Scholar] ; [View at Publisher].

[11] Hajimehrabi H, Behnamfar F, Samani AK, Goudarzi MA. Fragility curves for baffled concrete cylindrical liquid-storage tanks. Soil Dynamics and Earthquake Engineering. 2019 Apr 1;119:187-95. [View at Google Scholar] ; [View at Publisher].

[12] Rondon A, Guzey S. Brittle fracture assessment of the API specification 12F shop welded flat bottom tanks. International Journal of Pressure Vessels and Piping. 2017 Dec 1;158:69-78. [View at Google Scholar] ; [View at Publisher].

[13] Mebarki A, Jerez S, Prodhomme G, Reimeringer M. Natural hazards, vulnerability and structural resilience: tsunamis and industrial tanks. Geomatics, Natural Hazards and Risk. 2016 May 26;7(sup1):5-17. [View at Google Scholar] ; [View at Publisher].

[14] Saha SK, Matsagar VA, Jain AK. Reviewing dynamic analysis of base-isolated cylindrical liquid storage tanks under near-fault earthquakes. The IES Journal Part A: Civil & Structural Engineering. 2015 Jan 2;8(1):41-61. [View at Google Scholar] ; [View at Publisher].

[15] Miladi S, Razzaghi MS. Failure analysis of an un-anchored steel oil tank damaged during the Silakhor earthquake of 2006 in Iran. Engineering Failure Analysis. 2019 Feb 1;96:31-43. [View at Google Scholar] ; [View at Publisher].

[16] Celano F, Dolšek M. A simplified risk-targeted decision model for the verification of the seismic performance of critical infrastructure components to the operational limit state. Engineering Structures. 2020 Feb 1; 204:110019. [View at Google Scholar] ; [View at Publisher].

[17] Keramati M, Shariatmadari N, Karimpour-Fard M, Saeedanezhad A, Alidoust P. Effects of aging on dynamic properties of MSW: A case study from Kahrizak Landfill, Tehran, Iran. Sci. Iran. 2017. [View at Google Scholar] ; [View at Publisher].

[18] Alidoust P, Keramati M, Shariatmadari N. Laboratory studies on effect of fiber content on dynamic characteristics of municipal solid waste. Waste Management. 2018 Jun 1;76:126-37.[View at Google Scholar] ; [View at Publisher].

[19] Hou T, Wu XH, Cai Z. Convergence of a multiscale finite element method for elliptic problems with rapidly oscillating coefficients. Mathematics of computation. 1999;68(227):913-43. [View at Google Scholar] ; [View at Publisher].

[20] Pasquariello V, Hammerl G, Örley F, Hickel S, Danowski C, Popp A, Wall WA, Adams NA. A cut-cell finite volume–finite element coupling approach for fluid–structure interaction in compressible flow. Journal of Computational Physics. 2016 Feb 15;307:670-95. [View at Google Scholar] ; [View at Publisher].

[21] Deiterding R, Wood S. Parallel adaptive fluid–structure interaction simulation of explosions impacting on building structures. Computers & Fluids. 2013 Dec 15;88:719-29. [View at Google Scholar] ; [View at Publisher].

[22] Housner GW, Trifunac MD. Analysis of accelerograms—Parkfield earthquake. Bulletin of the seismological society of America. 1967 Dec 1;57(6):1193-220. [View at Google Scholar] ; [View at Publisher].

[23] Tinawi R, Léger P, Leclerc M, Cipolla G. Seismic safety of gravity dams: from shake table experiments to numerical analyses. Journal of Structural Engineering. 2000 Apr;126(4):518-29.[View at Google Scholar] ; [View at Publisher].